ISBN: 978-3-95450-232-5 ISSN: 2673-7000 doi:10.18429/JACoW-NAPAC2022-WEPA12

OPERATIONAL EXPERIENCE OF THE NEW BOOSTER CRYOMODULE AT THE UPGRADED INJECTOR TEST FACILITY*

M. Bruker†, R. Bachimanchi, J. Grames, M. McCaughan, J. Musson, P. Owen,
T. Plawski, M. Poelker, T. Powers, H. Wang, Y. Wang
Thomas Jefferson National Accelerator Facility, Newport News, VA, USA

Abstract

Since the early 1990s, the injector of the CEBAF accelerator at Jefferson Lab has relied on a normal-conducting RF graded-beta capture section to boost the kinetic energy of the electron beam from 100 / 130 keV to 600 keV for subsequent acceleration using a cryomodule housing two superconducting 5-cell cavities similar to those used throughout the accelerator. To simplify the injector design and improve the beam quality, the normal-conducting RF capture section and the cryomodule will be replaced with a new single booster cryomodule employing a superconducting, $\beta = 0.6$, 2-cell-cavity capture section and a single, $\beta = 0.97$, 7-cell cavity.

The Upgraded Injector Test Facility at Jefferson Lab is currently hosting the new cryomodule to evaluate its performance with beam before installation at CEBAF. While demonstrating satisfactory performance of the booster and good agreement with simulations, our beam test results also speak to limitations of accelerator operations in a noisy, thermally unregulated environment.

INTRODUCTION

In the interest of reducing space-charge-related beam-optical limitations as well as helicity-correlated variations of beam properties, the control of which is important for demanding parity-violation experiments such as MOLLER [1], the CEBAF injector at Jefferson Lab is undergoing a series of upgrades aiming to raise the initial beam energy to 200 keV and make the beam relativistic with as few extra elements as possible [2]. We are planning to replace the arrangement of capture section and double-five-cell SRF structure with a single compact SRF unit consisting of a pair of cavities: a new 2-cell capture cavity that provides a well-defined longitudinal focus for ballistic bunch compression upstream, and a C100-style 7-cell cavity to boost the energy [3, 4]. Table 1 lists the parameters, while Fig. 1 shows a model of the cryomodule.

Originally designed for a test of the HDIce in-beam cryostat [5] with a low-current electron beam at a maximum energy of 10 MeV, the Upgraded Injector Test Facility (UITF) is hosting the new booster cryomodule as its central element, allowing us to evaluate the performance of the device with beam prior to installing it in the CEBAF injector. The UITF gun operates at 180 kV, very close to the projected CEBAF value of 200 kV [6]. Figure 2 shows a schematic model of the beam line components relevant to this study.

Table 1: Nominal Parameters of the Booster Cryomodule

	2-cell	7-cell
Final kinetic beam energy (MeV)	0.533	5
Peak on-axis E field (MV m^{-1})		
nominal	4.6	13.2
maximum	8.0	26.0
Beam current (mA)		
nominal	0.38	
maximum	1.0	
Q_0 min.	4×10^9	8×10^9

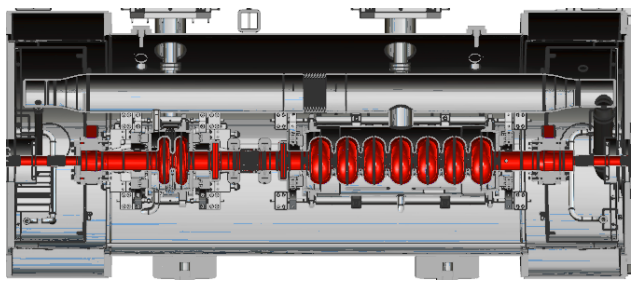

Figure 1: CAD model of the booster cryomodule excluding cryogenic attachments (cutplane view from the side; beam from left to right). The beam vacuum is highlighted in red, showing the 2-cell and the 7-cell cavity. Picture by J. Henry.

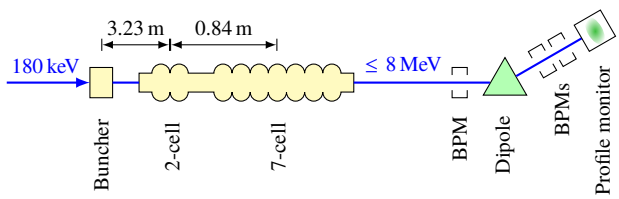

Figure 2: Relevant components of the beam line. A set of quadrupoles between booster and dipole (not shown) can be configured to provide a low β function at the diagnostic devices.

FIELD CALIBRATION

The dependency between energy gain and field amplitude of the booster has been the subject of many disagreements due to the non-relativistic velocity at the input, warranting a simulation study. While an empirical setup of the RF parameters based on the final beam momentum can be good enough

* This material is based upon work supported by the U.S. Department of Energy, Office of Science, Office of Nuclear Physics under contract DE-AC05-06OR23177.
† bruker@jlab.org

ISBN: 978-3-95450-232-5 ISSN: 2673-7000 doi:10.18429/JACoW-NAPAC2022-WEPA12

for undemanding experiments, systematically comparing such setups to simulations allows us to have confidence in the model and use it for predictive studies in the future.

The low-energy part of the beam line including the booster is modeled in GPT [7] using field maps of all elements computed with CST [8]. For these studies, we treat the longitudinal phase space in isolation and set all transverse components to zero; the longitudinal phase space is then observed downstream of the 7-cell cavity. In the corresponding experiment, the central momentum is determined by deflecting the beam by a known angle with a spectrometer dipole (see Fig. 2). First, we calibrate the arbitrary unit[1] of the field setpoint G_{set} against the physical peak field $A = \alpha G_{\text{set}}$ by optimizing α to give minimum-least-squares agreement between measured $E_{\text{kin,meas}}(G_{\text{set}})$ and simulated $E_{\text{kin,GPT}}(A)$. If the model is correct, the phases of maximum energy gain ϕ_{max} then have to agree for any field, allowing for a random phase offset between each RF device and the simulation model, which we also optimize. Figure 3 compares the simulated and measured values aligned in this way. While not a definitive verification of the model in every aspect, this comparison reveals no obvious errors. Note that the field design of the 2-cell cavity makes the achievable energy gain almost proportional to the field amplitude despite the variation in beam velocity, provided the phase is adjusted to compensate for time-of-flight differences.

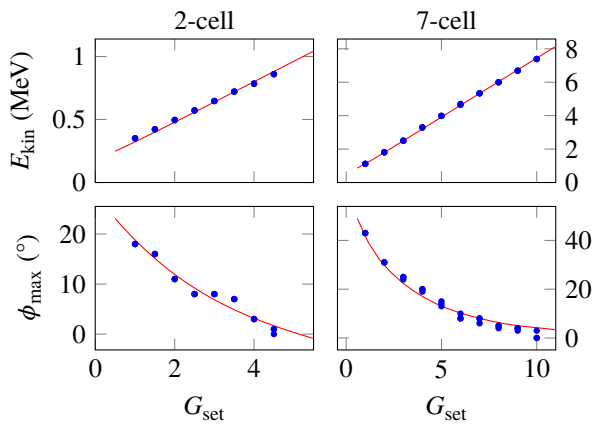

Figure 3: Empirical crest phase and total kinetic energy vs. field amplitude setpoint G_{set} (in control system units). The solid lines are GPT results scaled with $\alpha_{\text{2-cell}} = 2.017(15)\,\text{MV m}^{-1}$ and $\alpha_{\text{7-cell}} = 1.915(4)\,\text{MV m}^{-1}$. The phases have an arbitrary offset.

ENERGY SPREAD AND BUNCH LENGTH

As the 2-cell cavity is designed for an output velocity of $\beta \approx 0.9 \neq 1$, the question arises where exactly the longitudinal focus of the buncher should be and how to phase the other cavities. When operated at a negative phase relative to the RF crest, the 2-cell cavity can act as a second buncher. However, as a result of the extra energy spread incurred by bunching as well as RF curvature, the final energy spread $\sigma_E/\langle E\rangle$ and bunch length σ_t cannot be minimized independently, and the problem becomes one of multi-objective optimization.

Using the GPT model discussed above, we performed a minimization of the final bunch length and energy spread while reaching a fixed final energy of 8 MeV, which is currently the default beam energy for UITF experiments. The buncher is always operated at the bunching zero-crossing phase. For this precursory study, we used an initial RMS bunch length of 15 ps and no initial energy spread; space charge and transverse optics were also ignored. Under these idealized conditions, the Pareto front minimizing $\sigma_E/\langle E\rangle$ and σ_t in the $(A_{\text{buncher}}, A_{\text{2-cell}}, \phi_{\text{2-cell}}, A_{\text{7-cell}}, \phi_{\text{7-cell}})$ parameter space (A referring to peak field and ϕ to phase) is shown in Fig. 4.

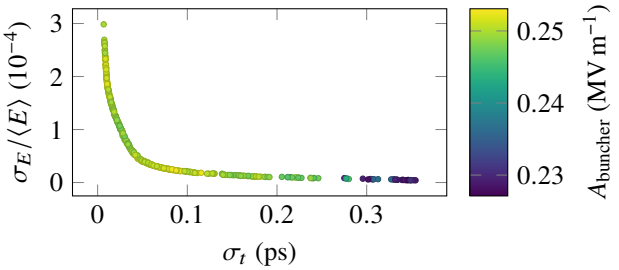

Figure 4: Pareto front for energy spread and bunch length. The point color denotes the peak buncher field.

The choice of buncher field suggested by the optimization results in slight overbunching at the 2-cell cavity; the optimal range of 2-cell phases is then centered around −40°. While these values give good results in practice, verifying their optimality in the machine is challenging for two reasons: there is presently no way to directly measure the bunch length, and the intrinsic energy spread of the bunches is swamped by amplitude and phase noise in the RF drive as discussed in the following section. For the time being, both booster cavities are operated at their respective phase of maximum energy gain.

FIELD STABILITY

An underappreciated consequence of the short bunch length and low momentum spread theoretically achievable with a short SRF booster is that temporal variations of phase or amplitude are comparatively impactful and easily become the performance bottleneck as experiments generally integrate the phase space over a length of time that is long compared to the RF period, effectively resulting in a larger phase space area. While these variations are mostly a result of external disturbances—most notably, microphonic detuning—and, as such, are attenuated by the negative-feedback loop around the cavity, the gain and bandwidth of the feedback are finite due to loop stability limits, resulting in a certain part of any disturbance ending up in the cavity field and,

[1] Per JLab convention, this unit should be MV m^{-1}, but that is not meaningful when dealing with a non-relativistic beam, so we will treat it as arbitrary for the sake of independent beam-based calibration.

ISBN: 978-3-95450-232-5 ISSN: 2673-7000 doi:10.18429/JACoW-NAPAC2022-WEPA12

consequently, the beam momentum. On the other hand, owing to the high Q of the cavities, modulation frequencies of more than a few hundred Hz cannot contribute meaningfully to the field acting on the beam.

The low-level-RF (LLRF) hardware [9] readily provides a downmixed field-probe signal to measure the AC components of the field; also, the beam momentum can be observed for comparison by recording the downmixed beam-position-monitor (BPM) signal in a dispersive location where the transverse beam motion ideally has no non-dispersive component. The measured beam position variation translates to an RMS momentum variation of $\delta p/p = 4 \times 10^{-4}$; at the same time, the RMS variation of relative cavity field amplitudes is 2×10^{-4} for the 2-cell and 5×10^{-4} for the 7-cell cavity. The latter number is an overestimate because of the white noise floor in the probe signal, which does not appear to be real.

Figure 5 shows the spectra of the beam and the cavities in comparison. With the exception of the mains-harmonic peaks, which are also present in the non-dispersive spectrum, the ratio between the two dispersive BPM signals is equal to the ratio between their dispersion values η, i.e., these spectra mostly contain momentum information. Expectedly, the spectral content of the cavity fields transfers to the beam and is predominantly microphonic in nature as shown by the detuning spectrum, driven by external vibration sources elsewhere in the building. The pink noise in the beam not present in the field probe spectrum is most likely due to phase noise from the oscillator.

Apart from noise on the beam momentum, reproducibility and long-term stability have also been observed to be an issue over the months. As the machine as a whole and the RF system in particular is subject to environmental conditions such as temperature, some drift is to be expected. Figure 6 shows the average beam position at non-dispersive and dispersive BPMs as a function of time. The drift of the non-dispersive beam position originates at the frontend and has yet to be investigated, making the dispersive data less conclusive. Nonetheless, comparing the curves shows that the beam momentum changes by at least several 10^{-4} over the course of hours.

One remaining issue not obvious from either the averaged spectra or the long-term beam position is periodic, sharp detuning transients of tens of degrees, threatening operational stability. Occurring every 5 min, they are assumed to be environmental; however, conclusive evidence of the source remains to be found.

Even with these disturbances, the short-term energy spread passes the design specification [3] of $\sigma_E/\langle E\rangle < 10^{-3}$; the specified bunch length limit $\sigma_t < 0.5$ ps, while not directly measurable at the UITF, is implicitly kept as well according to phase space simulations.

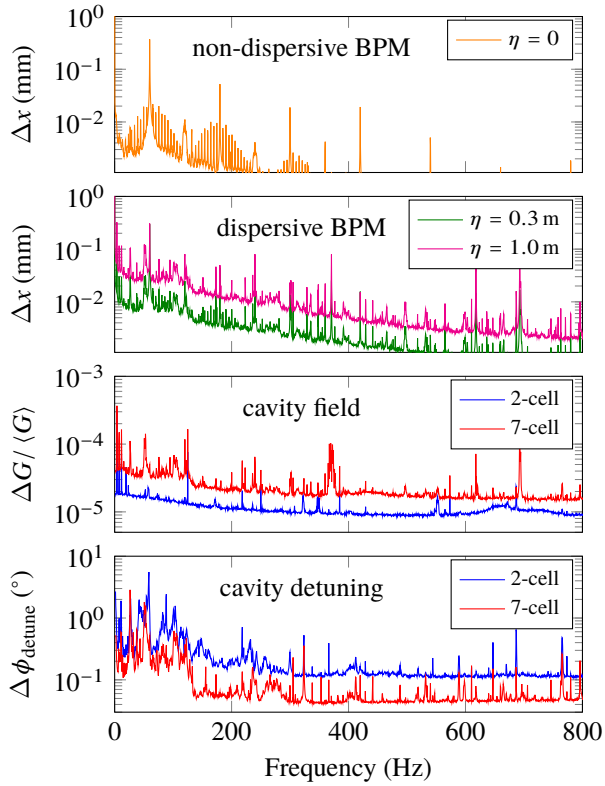

Figure 5: First and second plot: spectral content of transverse beam positions before and after the dipole, respectively. Third and fourth plot: field and detuning of the booster cavities.

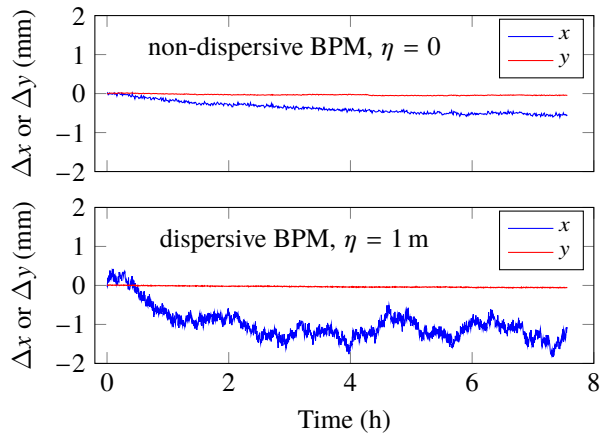

Figure 6: Long-term beam position drift on non-dispersive (top) and dispersive BPM (bottom).

CONCLUSION

The booster cryomodule has been tested extensively and is deemed fit for installation in the CEBAF injector, its performance within the specified limits to the extent measurable at the UITF. Seeing good agreement between simulation and beam-based setup, we are confident in our model, enabling predictions of the phase space. Although vibrations, thermal drifts, and other unresolved noise issues remain that are detrimental to UITF operations, they are attributed to the test facility and not expected to exist at CEBAF.

ISBN: 978-3-95450-232-5 ISSN: 2673-7000 doi:10.18429/JACoW-NAPAC2022-WEPA12

REFERENCES

[1] MOLLER Collaboration *et al.*, "The MOLLER Experiment: An Ultra-Precise Measurement of the Weak Mixing Angle Using Møller Scattering," 2014. doi:10.48550/ARXIV.1411.4088

[2] R. Kazimi, A. Freyberger, F. E. Hannon, A. S. Hofler, and A. Hutton, "Upgrading the CEBAF Injector with a New Booster, Higher Voltage Gun, and Higher Final Energy," in *Proc. IPAC'12*, New Orleans, LA, USA, May 2012, pp. 1945–1947.

[3] H. Wang *et al.*, "RF Design Optimization for New Injector Cryounit at CEBAF," in *Proc. IPAC'13*, Shanghai, China, May 2013, pp. 2471–2473.

[4] H. Wang *et al.*, "Injector Cavities Fabrication, Vertical Test Performance and Primary Cryomodule Design," in *Proc. IPAC'15*, Richmond, VA, USA, May 2015, pp. 3551–3553. doi:10.18429/JACoW-IPAC2015-WEPWI030

[5] C. Hanretty, "eHD at UITF", Hall B meeting, 2016. https://www.jlab.org/Hall-B/HDIce/talks/eHD_at_UITF_HallBMeeting.pdf

[6] J. M. Grames *et al.*, "CEBAF 200 kV Inverted Electron Gun," in *Proc. PAC'11*, New York, NY, USA, Mar.-Apr. 2011, pp. 1501–1503.

[7] Pulsar Physics, "General Particle Tracer", 2022. http://www.pulsar.nl/gpt

[8] CST Microwave Studio Suite, 2022. http://www.cst.com

[9] T. E. Plawski *et al.*, "JLAB LLRF 3.0 Development and Tests," in *Proc. IPAC'21*, Campinas, Brazil, May 2021, pp. 4340–4342. doi:10.18429/JACoW-IPAC2021-THPAB271